Ocean and Coastal Research

ORIGINAL ARTICLE

http://doi.org/10.1590/2675-2824072.24008
ISSN 2675-2824

Identifying the origins of nanoplastics in the abyssal South Atlantic using backtracking Lagrangian simulations with fragmentation

Claudio M. Pierard*[1], Florian Meirer[2], Erik van Sebille[1]

[1] Utrecht University – Institute for Marine and Atmospheric Research (Princetonplein 5, 3584 CC – Utrecht – Netherlands).
[2] Utrecht University – Debye Institute for Nanomaterials Science & Institute for Sustainable and Circular Chemistry, Inorganic Chemistry and Catalysis (Universiteitsweg 99, 3584 CG – Utrecht – Netherlands).

* Corresponding author: c.m.pierard@uu.nl

ABSTRACT

During an expedition in January 2019, nanoplastics were sampled at a depth of −5,170 m over Cape Basin, in the South Atlantic Ocean. Using photo-induced force microscopy, it was suggested that these were polyethylene terephthalate (PET-like) particles with various sizes down to 100 nm, at different stages of degradation. By using a state-of-the-art Lagrangian 3D model, which includes fragmentation, we backtracked virtual particles to map the origin of the PET nanoplastics sampled at this location. Fragmentation processes are crucial to understanding the origin of nanoplastics (and microplastics) because they allow for detecting when and where particles become so small that they transition to a colloidal state, in which the buoyant force becomes negligible. We found that it is very unlikely that the nanoplastic particles entered the ocean as nanoplastics and then drifted to the sampling location. We also found that the fragmentation scheme, particularly the fragmentation timescale prescribed to the modeled particles, affects how they drift in the ocean by the velocity with which they sink. This study contributes to understanding the fate and sources of nanoplastics in the deep ocean and the development of 3D backtracking simulations for source attribution of ocean plastic.

Keywords: Nanoplastics, Lagrangian, Fragmentation, Transport, Ocean

INTRODUCTION

Plastic is a pervasive pollutant that has reached some of the most remote ecosystems on Earth such as the deep ocean (Woodall et al., 2014, Chiba et al., 2018, Canals et al., 2021). Once they enter the ocean, bulk plastics start degrading by different weathering processes, such as UV radiation, mechanical abrasion, hydrolysis, and biodegradation (Alimi et al., 2018, Bond et al., 2018, Chamas et al., 2020). The degradation processes make the plastic items brittle, which fragment into microplastics and nanoplastics (Ter Halle et al., 2016, Lambert and Wagner, 2016, Gigault et al., 2021). Due to their small size and increased surface area-to-volume ratio, microplastics and nanoplastics act as vectors to transport contaminants like heavy metals (Brennecke et al., 2016, Rochman et al., 2014) and persistent organic pollutants (Bakir et al., 2014, Lee et al., 2014), which can harm marine

Submitted: 17-Jan-2024
Approved: 11-Jul-2024

Associate Editor: Cesar Rocha

organisms that ingest them (Rochman et al., 2013). Consequently, studying the transport of micro- and nanoplastics to remote and delicate ecosystems can be crucial to assessing their environmental impact. Compared to the microplastics floating at the ocean surface, the micro- and nanoplastics suspended in intermediate and deep waters remain understudied. Suspended microplastics have been sampled below and at the surface of the Atlantic Ocean, where the most common polymer types found were Polyethylene (PE), Polypropylene (PP), and Polystyrene (PS) particles, all positively buoyant (Pabortsava and Lampitt 2020, Poulain et al., 2019, Egger et al., 2020). Egger et al. (2020) measured the vertical distribution of plastic particles, from 500 µm to 5 cm in size, in the North Pacific Subtropical gyre, where they reported a power law decline with depth in the mass concentration of plastic. They found a positive correlation between the surface mass concentration and depth-integrated concentration at different locations. Moreover, they found that particles in the water column are in the size range and composition of particles missing from the ocean surface, indicating that they are most likely fallout from surface particles. In the South Atlantic, Zhao et al. (2022) sampled surface and water column microplastics at four locations in a transect going in and out of the South Atlantic Subtropical gyre. On average, they found a vertical decrease in particle abundance, with variations in the horizontal and vertical distributions of plastic particles < 100 µm. Of the particles detected in the water column, 65% were negatively buoyant and composed of high-density polymers.

From one of the samples collected at −5,170 m deep during the same expedition, Weckhuysen et al. (2021) detected PET-like nanoplastics down to < 100 nm in size seemingly at different stages of degradation by using photo-induced force microscopy. Their findings suggested that these particles could have originated from larger particles that fragmented into smaller particles while they were sinking or after being deposited on the seafloor. Assuming that most of the plastic enters the ocean through the surface or close to it, this study addresses the possible transport pathways of these nanoplastic particles towards the abyssal South Atlantic Ocean.

The fragmentation of plastics is a fundamental process to understand the transport of plastic in the ocean. Fragmentation changes the size and shape of particles, consequently changing the physical regime in which particles are transported. We defined these regimes by performing a scaling analysis for negatively buoyant spherical plastic particles from 0.01 µm to 100 µm in radius (see Text S1 and Table S1). From this analysis, we observe that for particles with $R < 1$ µm, the Brownian force dominates compared to the buoyant, inertial, and viscous forces (Gigault et al., 2021). Hence, particles with $R < 1$ µm are considered colloidal (Russel et al., 1989, Al Harraq and Bharti 2022), i.e., their buoyancy does not contribute to their vertical transport. For particles with $R > 1$ µm, the buoyant force dominates over the rest, thus, buoyancy starts to be relevant for their vertical transport. This size criterion matches the convention for the classification of nanoplastics proposed by the European Commission (2023) and Hartmann et al. (2019), which we used in this study to differentiate between passive particles or nanoplastics (1 nm to 1,000 nm) and buoyant particles or microplastics (1 µm to 1,000 µm).

Regarding the nanoplastics sampled in the abyssal South Atlantic, if the particles remained in a non-buoyant colloidal state during their journey from the surface to −5,170 m, we considered that they were transported by the ocean circulation, i.e., they followed the movement of the water masses. As an indicator, for water masses below −2,000 m in the mid-latitude South Atlantic, the mean time since these waters were last in contact with the surface is 460 ± 20 years (DeVries and Primeau, 2011, Primeau, 2005), despite a whole spectrum of water and tracer ages being present in a water parcel. In contrast, mass production of consumer plastics started after World War II (Geyer, 2020) and the presence of plastic in the geological records started in 1950 (Zalasiewicz et al., 2016). Thus, it is unlikely that colloidal particles were transported by the ocean circulation to where they were sampled because it would have taken the nanoplastics hundreds of years to do so.

As an alternative hypothesis, we here explore the possibility that the PET nanoplastics, found at the sampling location, fragmented from large parent particles that released nanoplastics and microplastics during their fallout, speeding up the transport of the nanoplastics to the deep ocean. The degradation of the parent particles might have been initiated at the surface by UV degradation and continued during the fallout by hydrolysis (Ioakeimidis et al., 2016, Sang et al., 2020). To test this hypothesis, we developed and performed a three-dimensional Lagrangian simulation in which we backtracked particles from the sampling location of the nanoplastics towards the possible sources at the surface, shedding light on the transport mechanisms and possible origins of nanoplastics in the deep ocean.

METHODS

Lagrangian Framework Set-Up

The hydrodynamic data used to advect the particles is the MOI_GLO12_WEEKLY_run_for_DAILY_FORECAST data from Mercator Ocean (2024). The MOI GLO12 data assimilates outputs from the Nucleus for European Modeling of the Ocean (NEMO v3.1 with the ORCA12 configuration; Madec et al., 2017), with observations via the Mercator Assimilation System 2 (SAM2), built around a Singular Evolutive Extended Kalman filter analysis kernel (SEEK; Tuan Pham et al., 1998). It contains the daily-averaged analysis and forecast Global Ocean Physics on a three-dimensional grid. The zonal, meridional, and vertical components of the velocity are on the native C-grid (no interpolation), with 1/12° horizontal resolution. In the vertical, the model has 50 z-coordinate levels with a scaled vertical grid spacing from −5,500 m to 0 m that concentrates the resolution near the ocean surface. The vertical resolution is 1 m at the surface, increasing to 95 m at −500 m and up to 448 m at the bottom. The bathymetry is represented with a partial cell. The MOI GLO12 data is provided as a daily means.

We performed Lagrangian simulations in a reverse-time mode (van Sebille et al., 2018), in which we advected virtual particles in the three-dimensional flow backward-in-time, combined with a vertical diffusion scheme that runs forward in time to represent unresolved convective motions. The particle trajectories were integrated using the OceanParcels framework v.2.4.2 (Delandmeter and van Sebille 2019) using a fourth-order Runge-Kutta integration time step of 1 h. We backtracked 8,192 virtual particles from the location where nanoplastics and microplastics were sampled (Weckhuysen et al., 2021, Zhao et al., 2022) to ensure statistically significant results. We created some variation in the trajectories by setting the 'initial' location of the particles to follow a horizontal normal distribution with its center at 32.171°S, 6.287°E, and a standard deviation of 0.01° To avoid the particles hitting the bottom boundary, the 'initial' depth of the particles was set to −5,000 m, on the second to last z-level grid cell (−5,052 m to −4,617 m), which is 180 m above the seafloor depth reported when sampling. All particles were backtracked for 12 years and 20 days, from January 20, 2019, to January 1, 2007. Each particle had an initial size randomly drawn from a uniform distribution ranging from 5×10^{-9} m to 5×10^{-7} m in radius and a constant density of 1,380 kg/m^3. It is important to highlight that the density of nanoplastics is unknown, but since buoyancy is negligible for particles in the nanoplastic size range, assuming a constant density do not affect their vertical transport. Also, the radius at which nanoplastics cease to be particles is still unknown.

Following Thygesen (2011) recommendations for performing a backward-in-time simulation in a three-dimensional domain, we backtracked the particles from the sampling location backward-in-time until they reached the surface, where we stopped backtracking them. The reason for stopping the backtracking of the particles at the surface is that when reversing the time in simulations for negatively buoyant particles, the particles will appear to 'rise' towards the surface. Once the particles reach the surface, they will continue to be forced upwards as we keep backtracking them, making them appear as if they were floating, although these particles are negatively buoyant. If we continue backtracking them after they reach the surface, until a time t_0, the particles will get dispersed by surface currents as if they were floating particles. On the contrary, if we perform

a forward-in-time simulation of the negatively buoyant particles, starting at their positions at t_0 obtained from the backward-in-time simulation, the particles will start sinking immediately to the seafloor, which will systematically under-represent the horizontal dispersion of the particles, creating a time asymmetry in the dispersion patterns between the backtracking and forward tracking simulations.

Regarding the seafloor or bottom boundary (where the vertical velocity w = 0), we reflected particles that hit the seafloor. We did not apply the same criterion as with the surface, given particles are constantly forced towards the surface because of the sinking velocity reversed in time. Therefore, if particles are released far from the bottom boundary, it is unlikely that they will hit the bottom boundary.

Sinking Velocity

This study concerns PET particles, which are denser than water, therefore, when submerged in the ocean, these particles sink. The sinking velocity v_s for the particles is defined as

$$v_s = \frac{2R^2 g(\beta - 1)}{9\nu} \quad (1)$$

in which R is the particle radius, g is the gravitational acceleration, ν is the kinematic viscosity of the fluid, and $\beta = \rho_p/\rho_f$ is the density ratio between the seawater ρ_p and the particle ρ_f. Eq. (1) is derived by assuming the plastic particles are spherical and there is a vertical force balance between the buoyancy force, their weight, and Stokes drag. Moreover, Eq. (1) is equivalent to the sinking velocity used by de la Fuente et al. (2021), Monroy et al. (2017), and Sutherland et al. (2023). Since we used Stokes drag to derive Eq. (1), we are assuming that particles are in a Stokesian regime, in which the particles Reynolds number $Re_p \ll 1$. The particle Reynolds number relates the inertial and viscous forces acting on the particle and it is defined as $Re_p \simeq v_s R/\nu$, in which v_s is the sinking velocity, R is the particle radius, and ν is the kinematic viscosity of the fluid.

Since fragmentation is considered in the simulations and the particle radius changes throughout the simulation, we defined the limit of validity of Eq. (1), which is given by the particle radius R and density ratio β, in which $Re_p \ll 1$. For PET particles of density 1,380 kg/m^3, immersed in the ocean water with a density ratio β = [1.31, 1.35], and assuming $\nu = 1.5 \times 10^{-6}$ m^2/s, R = 0.1 mm is the maximum limit of validity of Eq. (1). This limit is below the limit suggested by de la Fuente et al. (2021), in which the validity of the sinking velocity is defined by the Kolmogorov length scale in the ocean, with an estimated value of 0.3 mm in the ocean mixed layer.

For particles exceeding a radius of 0.1 mm, the sinking velocity predicted by Eq. (1) tends to be overestimated. This discrepancy is evident in Figure 1, in which the red curve illustrates the sinking velocity relative to the particle radius for particles with a buoyancy ratio of β = [1.31, 1.35]. The shaded area in grey denotes the region where R > 0.1 mm ($Re_p > 1$). Given that our simulations involve particles with R > 0.1 mm, we used the modified terminal velocity given by

$$v_s^* = \frac{v_s}{\mathcal{C}\left(Re_p\right)}, \quad \text{with} \quad \mathcal{C}\left(Re_p\right) = 1 + 0.15 Re_p^{0.687} \quad (2)$$

in which C is the Schiller–Naumann coefficient (Sutherland et al. 2023). The Schiller-Naumann coefficient is an empirical expression that corrects the drag coefficient function of spheres sinking in a $Re_p \ll 1$ regime to represent spheres sinking in a $Re_p < 800$ regime (Visuri et al., 2012). In Figure 1, the dashed blue line illustrates v_s*, showing that for particles in the $Re_p \ll 1$ regime (nanoplastics and small microplastics), v_s^* aligns with v_s. Meanwhile, for particles in the $Re_p > 1$ regime (large microplastics and mesoplastics), C adjusts the sinking velocity v_s^*, rectifying the overestimation introduced by Eq. (1).

Diffusion

To represent unresolved subgrid processes in the MOI GLO12 dataset that contribute to the dispersion of nanoplastics, such as convective motions and molecular diffusion, a vertical and an horizontal diffusion scheme were considered.

Regarding unresolved convective motions, we implemented a stochastic vertical random walk kernel using the vertical diffusion coefficients K_z from MOI GLO12 data, which is the background vertical eddy diffusivity that represents non-parameterized vertical mixing processes. The K_z field varies spatially and temporally in the domain; thus, to avoid accumulation of particles where the K_z gradients are high, we implemented a biased diffusive scheme, proposed by Ross and Sharples (2004), defined as

$$z(t-\Delta t) = z(t) + K_z'(z_t)\Delta t + B\sqrt{\frac{2K_z(\vec{x},t)\Delta t}{r}} - v_s^*\Delta t \quad (3)$$

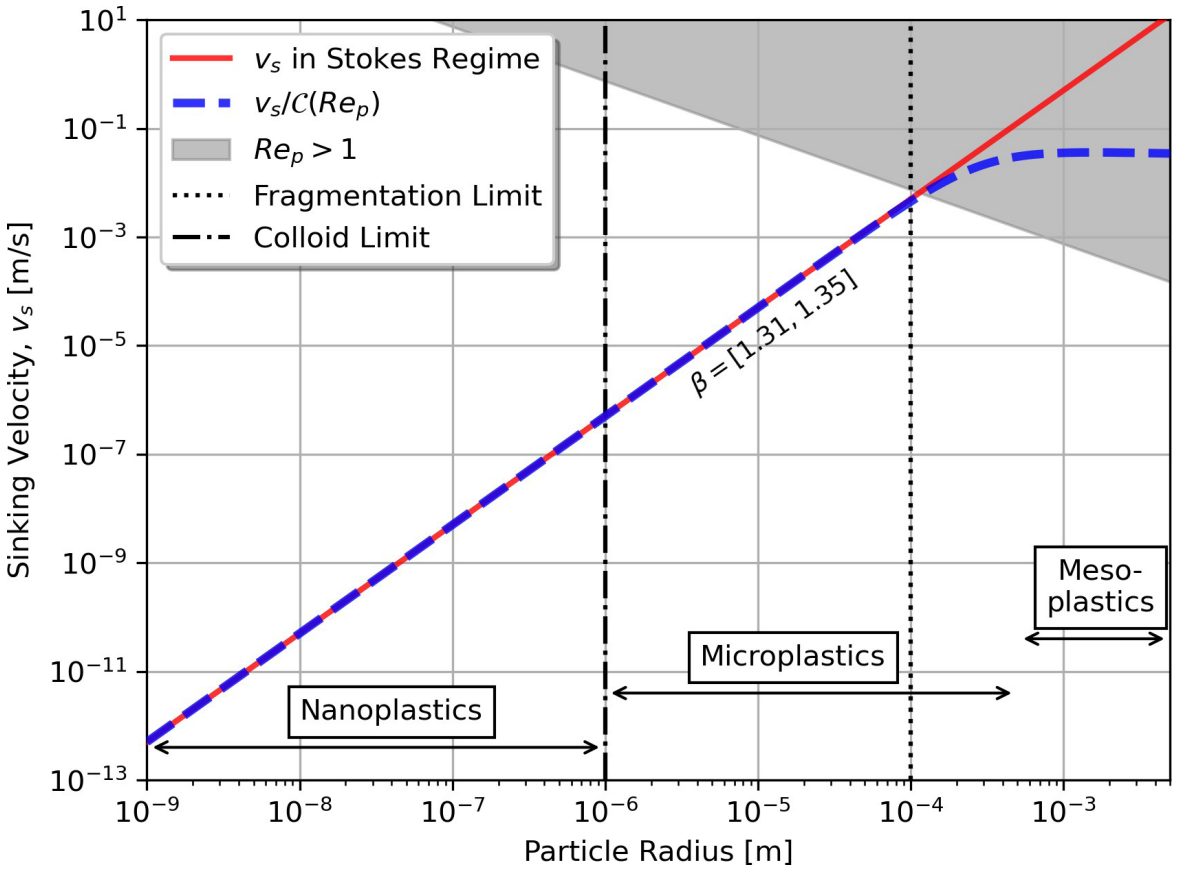

Figure 1. Sinking velocity computed with Eq.(1) for buoyancy ratios β = [1.31, 1.35] that correspond to PET particles submerged in stratified seawater. The shadowed grey area indicates the region where $Re_p > 1$. The red solid line represents the sinking velocity v_s given by Eq. (1). The black dotted line indicates the radius limit where the Eq. (1) is not valid anymore. The dashed-dotted line indicates the radius in which buoyancy does not contribute to the vertical transport of particles, i.e., the colloidal limit. The Blue dashed line shows the modified sinking velocity v_s^* given by Eq. (2). The nanoplastics radius range is defined as R = [1, 1,000]nm, the microplastics is defined as R = [1, 500]µm, and mesoplastics as R = [0.5, 2.5]mm.

in which z is the depth of the particles at a particular time, Δt is the timestep. On the right hand side of Eq. (3), the second term corresponds to the biased or deterministic term in which K_z' is the local vertical gradient of K_z around the particle position $\vec{x}$ at time t. The local K_z is linearly interpolated in the vertical to avoid sharp gradients when computing the local K_z'. According to Thygesen (2011), for heterogeneous turbulence in a backward-in-time simulation, this term should not be reversed or made negative to avoid particles accumulating in regions of low diffusion. The third

term corresponds to the random term, in which B is a random process generating numbers from [−1, 1] and r is the variance with a value of r = 1/3. The last term corresponds to the integration of the sinking velocity, in which v_s^* is the sinking velocity of the particle. Note that this term is reversed (i.e., made negative) because of the backwards-in-time scheme.

Molecular diffusion, a dominant force in the colloidal regime, can be represented as a horizontal random walk scheme by adding a stochastic term to the integration of the particle trajectory. For nanoplastics of R = 0.01 µm, submerged in water at 277.15 K, with dynamic viscosity η = 1.5 × 10^{-3} kg m^{-1} s, the molecular diffusivity is D_h = 1.56 × 10^{-6} m^2/s (Einstein, 1956, Kholodenko and Douglas 1995). For the simulation time span of 12 years, the root mean square displacement obtained by the random walk, with D_h, is equivalent to ∼ 24 m, which is insignificant compared to the thousands of kilometers the particles are dispersed by advection over the same time span. Therefore, on ocean scales, the contribution of molecular diffusion to the dispersion of particles is negligible compared to the dispersion done by the large scale and mesoscale dynamics, which are fully resolved in the MOI GLO12 dataset.

Regarding the representation of submesoscale processes occurring at spatial scales smaller than 1/12°, we did not incorporate a random walk scheme to represent the unresolved dynamics of the MOI GLO12 dataset. Representing Lagrangian submesoscale processes in ocean general circulation model simulation remains an active area of research, necessitating dynamically informed parametrizations beyond simple random walk schemes (Haza et al., 2012). The primary reason for this omission is that a random walk scheme would cause particles to jump in and out of eddy coherent structures present in the mesoscale field. It has been shown that the outer rim of quasi-coherent eddy structures are responsible for the bulk material transport of particles (Denes et al., 2022). Such imposed behavior could alter particle dispersion patterns, deviating from the mesoscale flow dispersion. On the other hand, implementing a simple random walk assumes a uniform diffusivity for the whole domain. However, a uniform diffusivity fails in capturing the mixing in areas with different eddy activity (van Sebille et al. 2020), variations that are present in a three dimensional eddy-resolving ocean general circulation model, such as in the MOI GLO12.

Kernel for Fragmentation Backwards in Time

We developed a fragmentation kernel that 'un-fragments' the virtual particles as we track them backward-in-time. Since time is reversed, the particles appear to grow at each fragmentation event as the simulation progresses. The fragmentation scheme is independent of the size of the particle and its numerical implementation consists of two steps.

The first step in the kernel controls when the fragmentation events occur. For this, we define a fragmentation probability p_f given by

$$p_f = 1 - e^{\frac{-|\Delta t|}{\lambda_f}} \tag{4}$$

in which Δt is the simulation timestep and λ_f is the fragmentation timescale or e-folding timescale (so that λ_f is the number of days that a particle has to be drifting to have a 63.2% chance of fragmenting).

The kernel performs a Bernoulli Trial in which, at every simulation timestep and for each particle individually, a probability p is randomly drawn from a uniform distribution and then compared to p_f. If $p > p_f$, then there is a fragmentation event for that particle. If $p < p_f$, then no fragmentation occurs in that timestep for that particle. The second step of the kernel determines how big the parent particle was before a fragmentation event. In a backwards-in-time simulation, when a fragmentation event occurs, we have to establish what size the parent particle of the fragmented particle was. We adapted the Turcotte (1986) and Kaandorp et al. (2021) fractal model to determine the size of the parent particle during a fragmentation event in our simulation. This model mimics the fragmentation of an object into a range of different-sized objects

in *one* event, which is intuitively like hitting a rock with a large hammer.

Similar to the idealized fragmentation model by Kaandorp et al. (2021), we assumed that a plastic particle resembles a cube of size L and mass M, and when (in forward-time) a fragmentation event occurs, the cube fragments into several smaller cubes of different size classes k with masses smaller than M. The number of cubes per size class in a fragmentation event depends on the mode of fragmentation m, which is the fraction of the mass in each size class that fragments into smaller size class particles. As an example, Figure 2 shows a parent particle during a single forward-time fragmentation event with m = 0.5, meaning that half of the mass of all the size classes is fragmented into smaller size class particles. In this example, we observe that a single fragmentation event creates half a cube of size class k = 0 with mass M/2, two cubes of size class k = 1 with a mass M/8 each, eight cubes size class k = 2 of mass M/64 each, 32 cubes size class k = 3 of mass M/512 each, and so on. In Figure 2, we grouped the cubes with the same size class to highlight that it is possible to reassemble the parent particle, with mass M and size class k = 0, by putting together all the fragments. The location where these particles come from the parent particle is irrelevant, we only care about the number of particles generated per size class and their mass relative to the parent particle.

The number of fragments per size class formed in a fragmentation event can be written as

$$n(k, m, D) = (1 - m)\,(2^{D}m)^{k} \qquad (5)$$

in which k is the size class, m is the fragmentation mode, and D is the dimensions of the particle. In this study, we consider three-dimensional objects (D = 3), but this fragmentation can also describe two-dimensional objects (D = 2) fragmentation such as plastic films (Kaandorp et al., 2021). The mass of a particle of a particular size class is given by $Mk = M_0/2^{kD}$, in which M_0 is the mass of the parent particle, k is the size class, and D is the fragmentation dimensions. We limited the kernel to only consider or track particles that fragmented into size classes $k \in [0, 1, 2, 3]$, ignoring size classes $k > 3$, to avoid particles to 'grow' infinitely (backwards in time). For the same reason, when the particles radius become larger than 0.1 mm we stopped them from un-fragmenting, making the size distribution at the end of the simulation to converge. This limit agrees with the limit of validity of Eq. (1).

In the Supplementary Material, Text S2 and Figure S2, we conducted a comparison of three simulations, each based on a distinct maximum size class k_{max}, with a constant λ_f set at 1,000 days.

The analysis revealed a reduction in both the time and the average number of fragmentation events required to go from the size distribution at the simulation's beginning (at the sampling location) to the size distribution at the end of the simulation. This reduction occurred when increasing the size classes considered to $k_{max} = 4$, as opposed to considering up to $k_{max} = 3$ classes. Conversely, limiting $k_{max} = 2$ had the opposite effect. Thus, altering the number of size classes had a comparable effect on modifying the fragmenting timescale λ_f, a parameter controlling the rate of particle fragmentation. To understand this influence, we conducted a sensitivity analysis, varying λ_f within the range of [100, 1,000, 10,000, 23,000] days. The degradation timescales $\lambda_f$considered correspond to an equivalent particle half-life ($t_{0,5} = \lambda_f \ln(2)$) of [0.19, 1.9, 19, 44] years, respectively. The λ_f = 23,000 days, matches the PET microplastics half-life (normalized to subtropical marine conditions) reported in accelerated degradation experiments in an UV chamber (Delre et al., 2023). Additionally, we considered shorter λ_f, based on the possibility that, due to their size, fragmentation timescales of nanoplastics may be faster compared to microplastic and bulk plastics estimates. We highlight, nevertheless, that there are no reported degradation rates for nanoplastics that support this hypothesis. The chosen values reflect the absence of standardized degradation rates for micro- and nanoplastics in marine environments, prompting us to define this range for a comprehensive understanding of how λ_f regulates particle transport.

The second step of the kernel consists of determining from which size class k ∈ [0, 1, 2, 3] the particle un-fragments into the parent particle. To determine this, we performed a random sampling of the size classes in which each size class has a size-independent probability based on the number of fragments per size class. This probability is given by

$$p_k(k,m) = \frac{n(k,m)}{\sum_{k_i=0}^{3} n(k_i,m)} \quad (6)$$

in which k is the size class, m is the fragmentation mass, and n(k, m) is the number of particles per

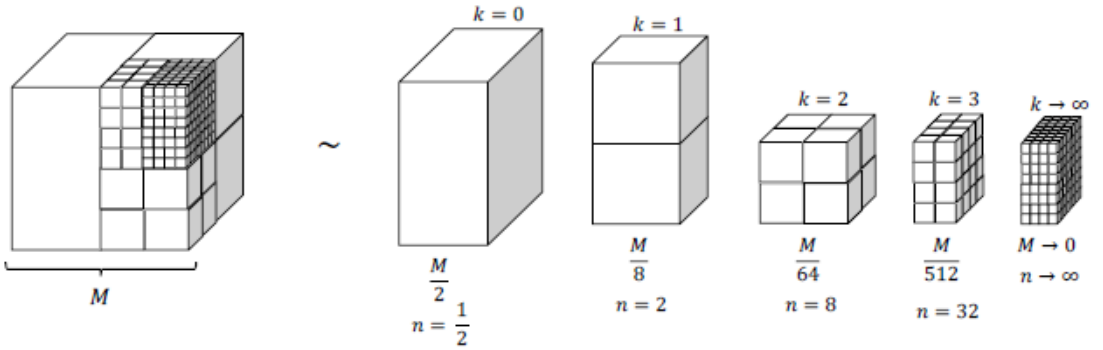

Figure 2. Diagram of a fragmentation event in forward-time. A cubic particle of mass M fragments into several smaller particles of different size classes: half a particle k = 0 with mass M/2, two k = 1 cubes with mass M/8, eight k = 2 cubes with mass M/64, and 32 k = 3 cubes with mass M/512. There is an infinite number of cubes of size classes smaller than k = 3.

size class. To illustrate this, based on Eq. (6), the probability of a particle un-fragmenting from a particle with mass M/2 to the parent particle with mass M (i.e., doubling its mass) is p_k (k=0, m=1/2) = 0.5/42.5 ≃ 0.01. The probability that the particle un-fragments from k = 1 to k = 0 (i.e. eight-fold increase in mass) is p_k (k=1, m=1/2) ≃ 0.05; the probability for the particle to un-fragment from k =2 to k =0 (i.e. 64 times its mass) is p_k (k=2, m=1/2) ≃ 0.19; and the probability of a particle to un-fragment from k =3 to k =0 (512 times its mass) is p_k (k=3, m=1/2) ≃ 0.75.

Therefore, when there is a fragmentation event, it is most likely that the particle will grow 512 times its mass. We set an upper size limit of 1×10^{-4} m at which particles stop un-fragmenting to prevent infinite 'growth' of particles. Particles below this limit can still un-fragment above this limit, but they still converge towards a radius below 1×10^{-3} m, as we limited the fragmenting size classes to k = 3.

To remain consistent with the assumption that particles are spherical, we computed an equivalent radius of the particles according to their mass. The equivalent radius of a cube particle with size L is $R = \sqrt[3]{3L^3/(4\pi)} = 0.62L$. In the case of the half k = 0 particle created in a fragmentation event, its equivalent radius is $R = \sqrt[3]{3L^3/(8\pi)} \simeq 0.49L$. When a particle un-fragments from a size class k = [1, 2, 3] to a size class k = 0, the new radius of the particle is given by

$$R_0(k) = \sqrt[3]{2^{kD} R_k^3} = 2^k R_k \quad (7)$$

in which R_0 is the radius of the particle after un-fragmenting, R_k is the radius of the particle before un-fragmenting, k is the size class, and D = 3. When a particle un-fragments from half a particle k = 0 to a complete particle, the new radius is given by

$$R_0 = \sqrt[3]{2R_{k=0}^3} \simeq 1.25R_{k=0} \quad (8)$$

To summarize, when there is a fragmentation event, particles will un-fragment into particles bigger than they were and, according to the second step of this kernel, it is most likely that the particle would increase 2^3 times its radius (k = 3 → 0) and less likely that it would grow 1.25 times its radius.

RESULTS

The surface as possible origin of PET Nanoplastics

Most particles backtracked from the sampling locations come from the ocean surface. In particular, all particles from simulations with λ_f =100 days reached the sampling location at –5,000 m from the ocean surface within the 12 years. For slower fragmenting timescales, such as λ_f = 1,000 days, λ_f = 10,000 days, and λ_f = 23,000 days, 86.3%, 4.3%, and 0.8% of particles came from the surface, respectively. The rest of the particles remained in intermediate waters during the 12 years of simulation.

Figure 3 shows the location at the surface where particles originated, shown as different markers and colors according to its λ_f. The star shows the location from where particles were backtracked. We found that the origin of the particles at the surface depends on the fragmentation timescale λ_f. For smaller λ_f, the origin position of particles is horizontally concentrated by a few hundred kilometers around the sampling location, compared to larger λ_f, where the origin is more dispersed. As a reference, the median horizontal displacement from the surface to the sampling location is below 1,000 km for all the λ_f considered. This means that, for half of the particles that came from the surface, the location where they started sinking can be traced back within a 1,000 km radius from the sampling location. However, the percentage of particles originating from distances smaller or equal to 1,000 km increases for the shorter degradation timescales considered.

As we see in Figure 3, most particles originating at the surface of the open ocean have their origin away from the coast. Only 0.08% of all particles, across all λ_f, originated within 100 km from the coast. In particular, all these particles had a λ_f = 1000 days, showing that if particles have fast fragmenting timescales, they would have sunk from relatively close distances from the sampling location. For the slower fragmenting timescales, it is more probable that the particles sunk away from the coastlines. The drift time that particles took to travel from the surface towards the sampling location was longer for particles with large fragmentation timescale. For instance, particles

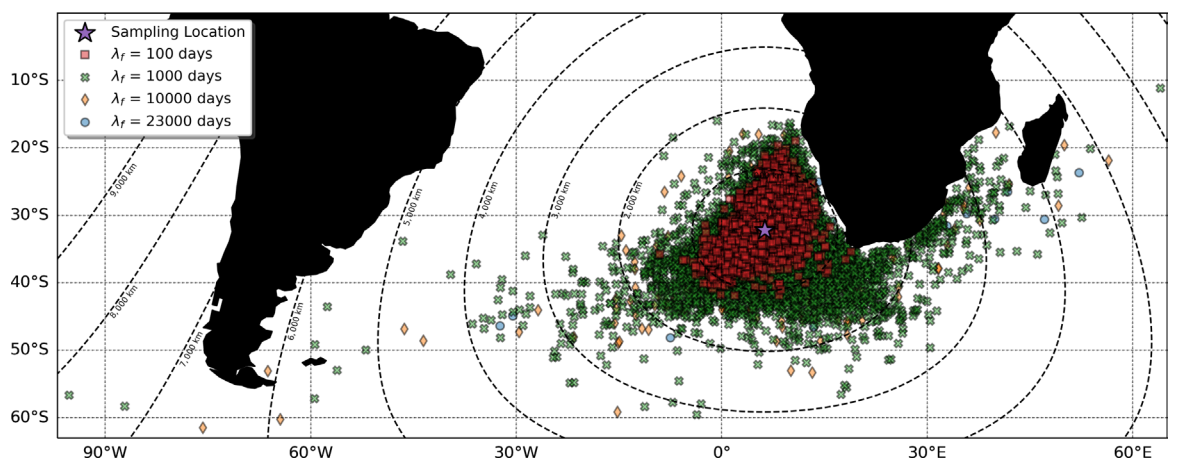

Figure 3. Map showing the probable origin of particles at the surface. The star shows the sampling location for the nanoplastics. Each marker and color show the locations for simulations with different fragmentation timescale λ_f. The black dashed lines show the equidistant lines from the sampling location, computed with the great circle distance, with 1,000 km between them.

with λ_f = 100 days had a median drift time of 310 days; particles with λ_f = 1,000 days had a median drift time of 5.9 years; for particles with λ_f = 10,000 days and λ_f = 23,000 days, the median drift time was around 8.5 years.

Figure 4 shows the empirical cumulative distributions of the particle radius at the surface, before sinking towards the sampling location. Each colored line represents the particles with different fragmentation timescales λ_f. We see that for all distributions, except λ_f = 10,000 days, the radius of particles is within the microplastics size range R > 1 µm. Regarding the λ_f = 10,000 days distribution, one out of 8,192 particles, reached the sampling location

starting its journey as a nanoplastic (with R < 1 µm). Also, we see that all the distributions overshoot from the radius limit (L = 1×10^{-4} m) imposed in the fragmentation kernel because particles that are near and below the radius limit are still able to un-fragment (backward-in-time) into larger particles exceeding the limit. Nevertheless, the upper bound for all distributions converges towards 1 × 10^{-3} m. The distributions are skewed towards bigger particles for fast fragmenting time scales, whereas the slower fragmenting timescales are skewed towards smaller particles. The skewness of the distributions is because, for faster fragmenting time scales, there are more particles overshooting the radius limit, thus the distributions have more bigger particles than the slower fragmenting time scales distributions.

Vertical Distribution of Nanoplastics

To understand if nanoplastics can form at the surface of the ocean and sink to –5,000 m, we filtered the trajectories of the particle when R < 1 µm, i.e., when they are nanoplastics and the buoyant forces do not dominate. We computed the probability of finding nanoplastics at a particular depth and time by binning the number of nanoplastic particles in bins of 100 m by 1 day for the entire water column

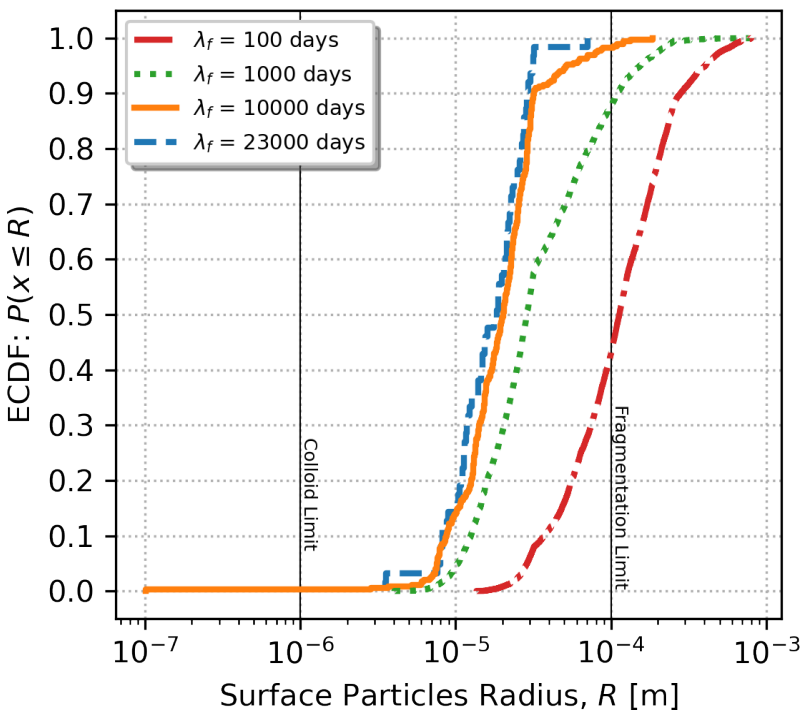

Figure 4. Empirical cumulative distribution functions (ECDF) of the particle size distribution of particles at the surface before being transported to the sampling location, according to its fragmentation timescale λ_f. The black vertical lines mark the 1 µm colloid limit for nanoplastics and the limit in which the fragmentation kernels stop un-fragmenting the particles.

and simulation time, then normalizing by the total number of nanoplastics in that day. Figure 5 shows in different panels the vertical probability distributions for finding particles with R < 1 µm at a specific day. Across all the fragmenting timescales, we see that a smaller fragmentation timescale λ_f results in less time for particles to drift as nanoplastics before reaching the sampling location. In particular, we see that for particles with $\lambda_f \leq$ 1,000 days, almost all the nanoplastics drift below –2,500 m in the 12 years before reaching the sampling location. We see that a small fraction of nanoparticles can drift from above –2,500 m towards the sampling location, but none of them can drift from the surface towards the sampling location. Regarding the λ_f = 10,000 days and λ_f = 23,000 days distribution, we see that the particle trajectories were more dispersed before 2014, showing particle trajectories above

the –2,500 m level. Due to their larger λ_f , particles cannot un-fragment from larger particles and most of them remain nanoplastics during the span of the simulation (backwards-in-time), thus the distribution is better represented. For λ_f = 10,000 days, only one particle

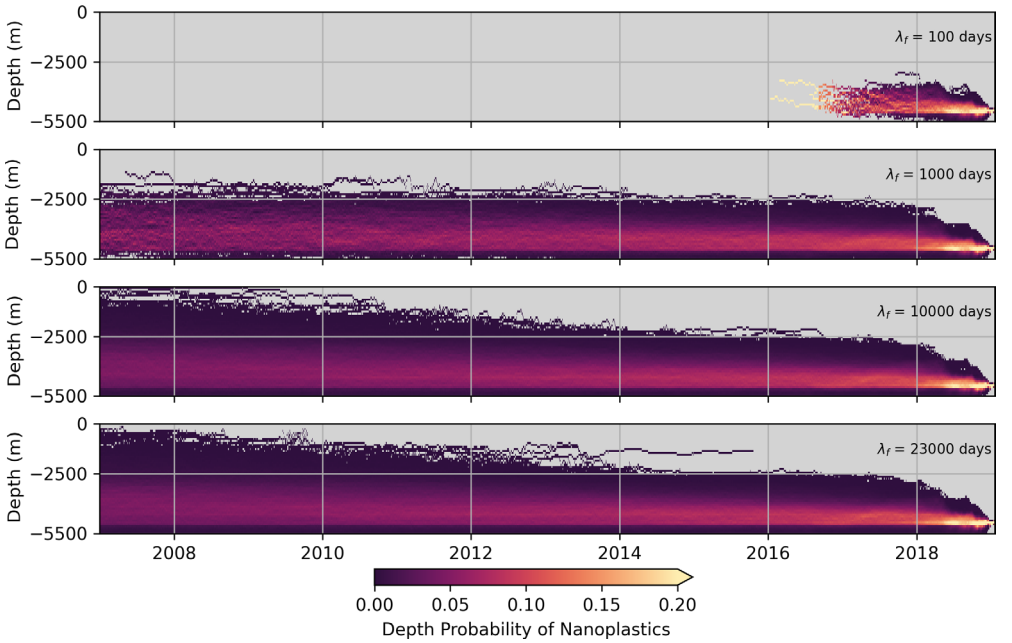

Figure 5. Figures showing the probability distributions of finding nanoplastics in the water column (from –5,500 m to 0 m deep) at a particular time throughout the simulation. The panels show the vertical distribution for a particular fragmenting timescale λ_f , arranged from fast (top) to slow (bottom). The color scale indicates the probability of nanoplastics present in a particular depth for a particular time. The grey shading indicates the absence of particles at that depth and time.

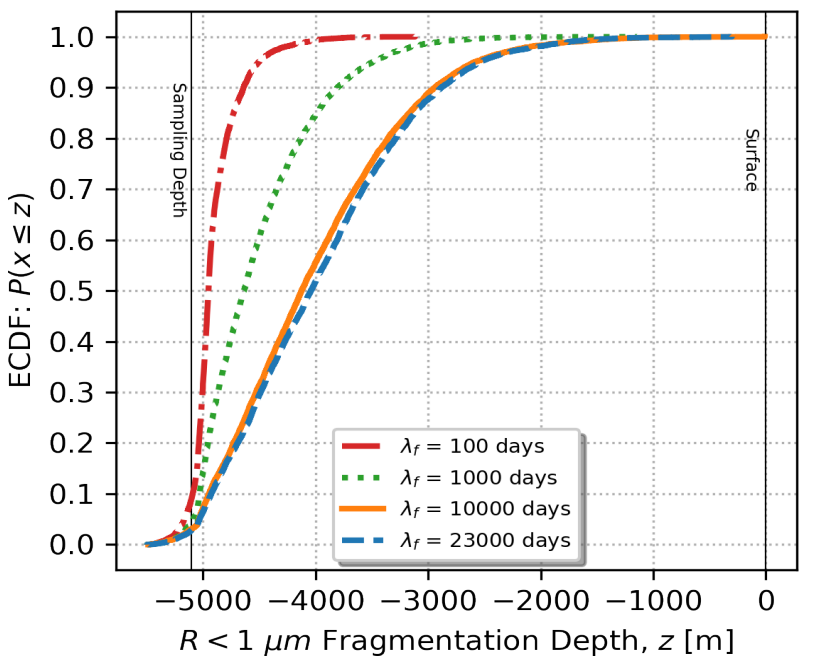

Figure 6. Empirical cumulative distribution functions (ECDF) of the depth where particles fragment into nanoplastics (R < 1 µm). Each fragmenting timescale λ_f is shown as a different color curve. The black vertical lines show the sampling location depth and the surface, respectively.

and 68% for λ_f = 100 days. In the region from 5,000 m to 5,500 m, the probability is ~ 7% for $\lambda_f \in [10{,}000, 23{,}000]$, 14% for λ_f = 1,000 days, and 31% for λ_f = 100 days. In Figure S2, in the Supplementary Material, we show a map of the locations where nanoplastics were formed.

DISCUSSION

As seen in Figure 6, it is unlikely but not impossible that PET nanoplastics (R < 1 μm) formed at the surface and then sank to −5,000 m. Theoretically, 1.32×10^{-5} m s^{-1} is the minimum sinking velocity needed for a particle to sink from the surface to −5,000 m in 12 years, assuming the ocean is completely still. Thus, from Eq.(1), the minimum radius, at any depth, for a particle to reach −5,000 m in less than 12 years, would range from 5.1×10^{-6} m to 5.42×10^{-6} m. Following this reasoning, it might be possible for nanoplastics to reach −5,000 m in 12 years. However, the ocean is in constant motion with dynamics at different length scales that can accelerate or decelerate their fallout.

As an alternative hypothesis is that nanoplastics fragmented from large parent particles that released nanoplastics and microplastics during their fallout. The fragmentation could have happened in several events and the fragmentation of the particles might have been initiated at the surface by UV degradation and continued during the fallout by hydrolysis (Ioakeimidis et al. 2016, Sang et al. 2020). Our results suggest that fragmentation is a key factor that might explain the presence of nanoplastics in the abyssal ocean. In the 12 years of simulations, we demonstrated that, for the slowest fragmentation timescales considered in this study, λ_f = 10,000 days and λ_f = 23,000 days, the most probable origin of nanoplastics remains the deep ocean (< −2,500 m). Nevertheless, we believe that by extending the simulation time beyond 12 years, the likelihood of nanoplastics originating at the surface would most likely increase.

For shorter degradation timescales, it is more evident that the nanoplastics found in the abyssal South Atlantic must have fragmented in the vicinity of the sampling location, and most likely in Cape Basin, the same region where nanoplastics were sampled. For small degradation timescales, the particles had to start their fallout as microplastics (R > 1 μm) to reach the sampling location. It is impossible for particles fragmenting at a $\lambda_f \leq 1{,}000$ days to reach −5,000 m. Regarding the location at the surface where particles started their fallout, we found that half of the particles could be traced back within a 1,000 km radius, as seen in Figure 3. The Namib desert is the nearest coast, located approximately 1,000 km away from the sampling location. This suggests that for fast degradation timescales, it is most likely that particles started their fallout in the open ocean rather than in coastal regions. However, we stopped the backtracking when particles reached the surface (in a backward-in-time scheme) because the negatively buoyant particles are constantly forced towards the surface, changing their dynamics (Thygesen 2011). This is a limitation for three-dimensional backtracking of PET particles, in which we can only establish the location where the particles started sinking from the surface.

We acknowledge the potential asymmetry between forward-tracking and backtracking simulations, particularly concerning the behavior of fragmenting negatively buoyant particles. This asymmetry becomes evident when comparing a forward-tracking simulation of microplastics (R≥1μm) fragmenting forward in time from the surface with a backtracking simulation of nanoplastics (R≤1μm) un-fragmenting backward in time from the sampling location. These two cases cannot be compared expecting the same outcomes. In a forward-in-time scheme, releasing particles as microplastics results in particles with small λ_f fragmenting rapidly into nanoplastics, becoming colloidal somewhere in the water column. We expect that none or a few of these particles will reach the sampling location, while the majority will become nanoplastics closer to the surface or sink to the ocean floor before becoming nanoplastics. For longer timescales, starting as microplastics from the surface, most particles will first hit the ocean floor before fragmenting into nanoplastics, never reaching the sampling location (assuming resuspension is ignored). In contrast, the backtracking simulation imposes the condition that all particles reach the sampling location as

nanoplastics. We explore possible trajectories that could have brought the particles to the sampling location under these imposed conditions. We then analyze which of these trajectories represent possible origins for the particles. For nanoplastics found at the sampling location, we assume the only origin of plastic is the surface, and the particles could have originated from the surface as either microplastics or nanoplastics. To understand the dynamics and possible dispersion of PET microplastics near the surface or in the mixed layer, a forward-in-time simulation would be necessary.

In general, it is difficult to prescribe the best fragmentation timescale for PET particles fragmenting under environmental conditions due to the lack of reported and standardized degradation rates of nanoplastics or microplastics under marine environments (Chamas et al., 2020). Also, the variability of degradation mechanisms depending on the various regions of the ocean makes prescribing a fragmentation timescale more challenging. According to Müller et al. (2001), the generally predicted lifetime of PET ranges from 16 to 48 years, suggesting that PET might be persistent in the environment.

However, considering the dark and cold conditions found in the deep ocean, the expected half-life of particles might be longer than the longest fragmentation timescale considered of λ_f =23,000 days. Even if we considered a greater fragmentation timescale than λ_f = 23,000 days, we would not expect to have very different results for the 12 years of simulations. The results would be similar to λ_f = 23,000 days and λ_f = 10,000 days, as almost all particles fragment only a few times in 12 years, making them remain in the colloidal regime, preventing them to reach the surface. It is necessary to perform longer than 12 years simulations to allow particles with a longer fragmenting timescale to reach the surface. This requires the use of longer datasets with velocity fields going further into the past with similar characteristics to the MOI GLO12 dataset.

The region from −5,000 m to −4,000 m, where most of the particles fragment into nanoplastics drifting towards the sampling location, has the coarsest vertical resolution in the MOI GLO12 velocity fields. The coarse resolution overlooks the dynamics occurring close to the deep seafloor that stirs, settles, and re-suspends material that drifts close to the seafloor, potentially affecting the dispersion of deep nanoplastics. By considering models with a better representation of these processes at the deepest grid cells, we believe that the dispersion patterns would change and more analysis could be performed, for example, estimating areas of potential resuspension of particles as probable sources of nanoplastics.

CONCLUSION

Fragmentation of plastic particles is crucial to simulate the transport of nano- and microplastics in the ocean, especially nanoplastics originating from indirect sources, like fragmentation from bulk plastics or microplastics. By including fragmentation in three-dimensional backtracking Lagrangian simulations, it is possible to estimate the regions in the ocean where these nanoplastics originate according to where they have been sampled in the environment. Notably, this fragmentation changes the particle size, transitioning from a buoyant to a colloidal regime, thereby modifying its vertical dynamics.

By focusing on the vertical distribution of the particles after backtracking, we concluded that nanoplastics with short fragmentation timescales, such as λ_f = 100 days and λ_f = 1,000 days, could not sink from the surface starting as nanoplastics and reach the sampling location at −5,000 m deep. Contrary to this, for the longer fragmentation timescales considered, λ_f = 10,000 days and λ_f = 23,000 days, this scenario is possible but highly unlikely within the 12 years considered.

Understanding the degradation rates of nanoplastics in the ocean environment is a priority, as it can inform whether nanoplastics are fast to degrade or whether they accumulate in the marine environment for decades. Quantifying the fragmentation timescales requires more experimental data for nanoplastics with different polymer compositions and under varying environmental conditions. This data would significantly enhance the models for degradation and fragmentation of nano- and microplastics, which in turn would improve the transport simulations.

SUPPORTING INFORMATION

The code and scripts are available at https://github.com/OceanParcels/Backtracking_Abyssal_Nanoplastics.git and https://zenodo.org/records/13366084

ACKNOWLEDGMENTS

We thank Mikael Kaandorp for his insights about plastic fragmentation that helped in the development phase of the fragmentation kernel. To Daan Reijnders for his insights on Lagrangian diffusivity that helped improve the diffusive kernels.

This project was supported by NWO through grant OCENW.GROOT.2019.043.

AUTHOR CONTRIBUTIONS

C.M.P.: Conceptualization; Investigation; Writing – original draft; Simulations; Formal Analysis; Investigation.

F.M.: ; Writing – review & editing; Supervision.

E.v.S.: Conceptualization; Writing – review & editing; Supervision.

REFERENCES

Al Harraq, A. & Bharti, B. 2022. Microplastics through the Lens of Colloid Science. *ACS Environmental Au*, 2(1), 3–10. DOI: https://doi.org/10.1021/acsenvironau.1c00016

Alimi, O. S., Farner Budarz, J., Hernandez, L. M. & Tufenkji, N. 2018. Microplastics and Nanoplastics in Aquatic Environments: Aggregation, Deposition, and Enhanced Contaminant Transport. *Environmental Science & Technology*, 52(4), 1704–1724. DOI: https://doi.org/10.1021/acs.est.7b05559

Bakir, A., Rowland, S. J. & Thompson, R. C. 2014. Transport of persistent organic pollutants by microplastics in estuarine conditions. *Estuarine, Coastal and Shelf Science*, 140, 14–21. DOI: https://doi.org/10.1016/j.ecss.2014.01.004

Bond, T., Ferrandiz-Mas, V., Felipe-Sotelo, M. & Van Sebille, E. 2018. The occurrence and degradation of aquatic plastic litter based on polymer physicochemical properties: A review. *Critical Reviews in Environmental Science and Technology*, 48(7-9), 685–722. DOI: https://doi.org/10.1080/10643389.2018.1483155

Brennecke, D., Duarte, B., Paiva, F., Caçador, I. & Canning-Clode, J. 2016. Microplastics as vector for heavy metal contamination from the marine environment. *Estuarine, Coastal and Shelf Science*, 178, 189–195. DOI: https://doi.org/10.1016/j.ecss.2015.12.003

Canals, M., Pham, C. K., Bergmann, M., Gutow, L., Hanke, G., Sebille, E. V., Angio-Lillo, M., Buhl-Mortensen, L., Cau, A., Ioakeimidis, C., Kammann, U., Lundsten, L., Papatheodorou, G., Purser, A., Sanchez-Vidal, A., Schulz, M., Vinci, M., Chiba, S., Galgani, F., Langenkämper, D., Möller, T., Nattkemper, T. W., Ruiz, M., Suikkanen, S., Woodall, L., Fakiris, E., Jack, M. E. M. & Giorgetti, A. 2021. The quest for seafloor macrolitter: a critical review of background knowledge, current methods and future prospects. *Environmental Research Letters*, 16(2), 023001. DOI: https://dx.doi.org/10.1088/1748-9326/abc6d4

Chamas, A., Moon, H., Zheng, J., Qiu, Y., Tabassum, T., Jang, J. H., Abu-Omar, M., Scott, S. L. & Suh, S. 2020. Degradation Rates of Plastics in the Environment. *ACS Sustainable Chemistry & Engineering*, 8(9), 3494–3511. DOI: https://doi.org/10.1021/acssuschemeng.9b06635

Chiba, S., Saito, H., Fletcher, R., Yogi, T., Kayo, M., Miyagi, S., Ogido, M. & Fujikura, K. 2018. Human footprint in the abyss: 30 year records of deep-sea plastic debris. *Marine Policy*, 96, 204–212. DOI: https://doi.org/10.1016/j.marpol.2018.03.022

de la Fuente, R., Drótos, G., Hernández-García, E., López, C. & Van Sebille, E. 2021. Sinking microplastics in the water column: simulations in the Mediterranean Sea. *Ocean Science*, 17(2), 431–453. DOI: https://doi.org/10.5194/os-17-431-2021

Delandmeter, P. & Van Sebille, E. 2019. The Parcels v2.0 Lagrangian framework: new field interpolation schemes. *Geoscientific Model Development*, 12(8), 3571–3584. DOI: https://doi.org/10.5194/gmd-12-3571-2019

Delre, A., Goudriaan, M., Morales, V. H., Vaksmaa, A., Ndhlovu, R. T., Baas, M., Keijzer, E., De Groot, T., Zeghal, E., Egger, M., Röckmann, T., Niemann, H. 2023. Plastic photodegradation under simulated marine conditions. *Marine Pollution Bulletin*, 187, 114544. DOI: https://doi.org/10.1016/j.marpolbul.2022.114544

Denes, M. C., Froyland, G. & Keating, S. R. 2022. Persistence and material coherence of a mesoscale ocean eddy. *Physical Review Fluids*, 7(3), 034501.

DeVries, T. & Primeau, F. 2011. Dynamically and Observationally Constrained Estimates of Water-Mass Distributions and Ages in the Global Ocean. *Journal of Physical Oceanography,* 41(12), 2381–2401. DOI: https://doi.org/10.1175/JPO-D-10-05011.1

Egger, M., Sulu-Gambari, F. & Lebreton, L. 2020. First evidence of plastic fallout from the North Pacific Garbage Patch. *Scientific Reports*, 10(1): 7495. DOI: https://doi.org/10.1038/s41598-020-64465-8

Einstein, A. 1956. *Investigation on the Theory of Brownian Movement edited by R. Furth*. New York, Dover.

European Comission. 2023. *Nanoplastics: state of knowledge and environmental and human health impacts*. Luxembourg, Publications Office of the European Union.

Geyer, R. 2020. A Brief History of Plastics. In: Streit-Bianchi, M, Cimadevila, M. & Trettnak, W. (eds.). *Mare Plasticum - The Plastic Sea: Combatting Plastic Pollution Through Science and Art* (pp. 31–47). Cham: Springer International Publishing.

Gigault, J., El Hadri, H., Nguyen, B., Grassl, B., Rowenczyk, L., Tufenkji, N., Feng, S. & Wiesner, M. 2021. Nanoplastics are neither microplastics nor engineered nanoparticles. *Nature Nanotechnology*, 16(5), 501–507. Number: 5 Publisher: Nature Publishing Group. DOI: https://doi.org/10.1038/s41565-021-00886-4

Hartmann, N. B., Hüffer, T., Thompson, R. C., Hassellöv, M., Verschoor, A., Dau-Gaard, A. E., Rist, S., Karlsson,

T., Brennholt, N., Cole, M., Herrling, M. P., Hess, M. C., Ivleva, N. P., Lusher, A. L. & Wagner, M. 2019. Are We Speaking the Same Language? Recommendations for a Definition and Categorization Framework for Plastic Debris. *Environmental Science & Technology*, 53(3), 1039–1047. DOI: *https://doi.org/10.1021/acs.est.8b05297*

Haza, A. C., Özgökmen, T. M., Griffa, A., Garraffo, Z. D. & Piterbarg, L. 2012. Parameterization of particle transport at submesoscales in the gulf stream region using lagrangian subgridscale models. *Ocean Modelling*, 42, 31–49.

Ioakeimidis, C., Fotopoulou, K. N., Karapanagioti, H. K., Geraga, M., Zeri, C., Papathanassiou, E., Galgani, F. & Papatheodorou, G. 2016. The degradation potential of PET bottles in the marine environment: An ATR-FTIR based approach. *Scientific Reports*, 6(1): 23501. https://doi.org/10.1038/srep23501

Kaandorp, M. L. A., Dijkstra, H. A. & Sebille, E. V. 2021. Modelling size distributions of marine plastics under the influence of continuous cascading fragmentation. *Environmental Research Letters*, 16(5), 054075. DOI: https://dx.doi.org/10.1088/1748-9326/abe9ea

Kholodenko, A. L. & Douglas, J. F. 1995. Generalized Stokes-Einstein equation for spherical particle suspensions. *Physical Review E*, 51(2), 1081–1090. DOI: https://doi.org/10.1103/PhysRevE.51.1081

Lambert, S. & Wagner, M. 2016. Formation of microscopic particles during the degradation of different polymers. *Chemosphere*, 161, 510–517. DOI: https://doi.org/10.1016/j.chemosphere.2016.07.042

Lee, H., Shim, W. J. & Kwon, J.-H. 2014. Sorption capacity of plastic debris for hydrophobic organic chemicals. *Science of The Total Environment*, 470-471: 1545–1552. DOI: https://doi.org/10.1016/j.scitotenv.2013.08.023

Madec, G., Bourdallé-Badie, R., Bouttier, P.-A., Bricaud, C., Bruciaferri, D., Calvert, D., Chanut, J., Clementi, E., Coward, A., Delrosso, D., Ethé, C., Flavoni, S., Graham, T., Harle, J., Iovino, D., Lea, D., Lévy, C., Lovato, T., Martin, N., Masson, S., Mocavero, S., Paul, J., Ousset, C., Storkey, D., Storto, A. & Vancoppenolle, M. 2017. *NEMO ocean engine*. France, Institut Pierre-Simon Laplace. Available from**:** *https://www.earth-prints.org/handle/2122/13309* Access date: 23 jul. 2024.

Mercator Ocean. 2024. *MOI GLO 12*. Toulouse, Mercator Ocean International. Available from: https://www.mercator-ocean.eu/en/solutions-expertise/accessing-digital-data/product-details/?offer=4217979b-2662-329a-907c-602fdc69c3a3&system=d35404e4-40d3-59d6-3608-581c9495d86a. Access date: 2024 Abr. 09.

Monroy, P., Hernández-García, E., Rossi, V. & López, C. 2017. Modeling the dynamical sinking of biogenic particles in oceanic flow. *Nonlinear Processes in Geophysics*, 24(2), 293–305. DOI: https://npg.copernicus.org/articles/24/293/2017

Müller, R.-J., Kleeberg, I. & Deckwer, W.-D. 2001. Biodegradation of polyesters containing aromatic constituents. *Journal of biotechnology*, 86(2), 87–95.

Pabortsava, K. & Lampitt, R. S. 2020. High concentrations of plastic hidden beneath the surface of the Atlantic Ocean. *Nature Communications*, 11(1), 4073. Doi: https://doi.org/10.1038/s41467-020-17932-9

Poulain, M., Mercier, M. J., Brach, L., Martignac, M., Routaboul, C., Perez, E., Desjean, M. C. & Ter Halle, A. 2019. Small Microplastics As a Main Contributor to Plastic Mass Balance in the North Atlantic Subtropical Gyre. *Environmental Science & Technology*, 53(3), 1157–1164. DOI: https://doi.org/10.1021/acs.est.8b05458

Primeau, F. 2005. Characterizing Transport between the Surface Mixed Layer and the Ocean Interior with a Forward and Adjoint Global Ocean Transport Model. *Journal of Physical Oceanography* 35(4): 545–564. DOI: https://doi.org/10.1175/JPO2699.1

Rochman, C. M., Browne, M. A., Halpern, B. S., Hentschel, B. T., Hoh, E., Karapanagioti, H. K., Rios-Mendoza, L. M., Takada, H., Teh, S. & Thompson, R. C. 2013. Classify plastic waste as hazardous. *Nature*, 494(7436), 169–171. DOI: https://doi.org/10.1038/494169a

Rochman, C. M., Hentschel, B. T. & Teh, S. J. 2014. Long-Term Sorption of Metals Is Similar among Plastic Types: Implications for Plastic Debris in Aquatic Environments. *PLOS ONE,* 9(1), e85433. DOI: https://doi.org/10.1371/journal.pone.0085433

Ross, O. N. & Sharples, J. 2004. Recipe for 1-D Lagrangian particle tracking models in space-varying diffusivity. *Limnology and Oceanography: Methods*, 2(9), 289–302. DOI: https://doi.org/10.1371/journal.pone.0085433

Russel, W. B., Saville, D. A. & Schowalter, W. R. 1989. *Colloidal Dispersions*, Cambridge Monographs on Mechanics. Cambridge, Cambridge University Press**.**

Sang, T., Wallis, C. J., Hill, G. & Britovsek, G. J. P. 2020. Polyethylene terephthalate degradation under natural and accelerated weathering conditions. *European Polymer Journal*, 136, 109873. DOI: https://doi.org/10.1016/j.eurpolymj.2020.109873

Sutherland, B. R., Dibenedetto, M., Kaminski, A. & van den Bremer, T. 2023. Fluid dynamics challenges in predicting plastic pollution transport in the ocean: A perspective. *Physical Review Fluids*, 8(7), 070701. Publisher: American Physical Society. DOI: https:doi.org/10.1103/PhysRevFluids.8.070701

Ter Halle, A., Ladirat, L., Gendre, X., Goudouneche, D., Pusineri, C., Routaboul, C., Tenailleau, C., Duployer, B. & Perez, E. 2016. Understanding the Fragmentation Pattern of Marine Plastic Debris. *Environmental Science & Technology*, 50(11), 5668–5675. DOI: https://doi.org/10.1021/acs.est.6b00594

Thygesen, U. H. 2011. How to reverse time in stochastic particle tracking models. *Journal of Marine Systems*, 88(2),159–168. DOI: https://doi.org/10.1016/j.jmarsys.2011.03.009

Tuan Pham, D., Verron, J. & Christine Roubaud, M. 1998. A singular evolutive extended Kalman filter for data assimilation in oceanography. *Journal of Marine Systems*, 16(3), 323–340. DOI: https://doi.org/10.1016/S0924-7963(97)00109-7

Turcotte, D. L. 1986. Fractals and fragmentation, *Journal of Geophysical Research: Solid Earth*, 91(B2), 1921–1926. DOI: https://doi.org/10.1029/JB091iB02p01921

van Sebille, E., Aliani, S., Law, K. L., Maximenko, N., Alsina, J. M., Bagaev, A., Bergmann, M., Chapron,

B., Chubarenko, I., Cózar, A., Delandmeter, P., Egger, M., Fox-Kemper, B., Garaba S. P., Goddijn-Murphy, L., Hardesty B. D., Hoffman M. J., Isobe, A., Jongedijk, C. E., Kaandorp, M. L., A., Khatmullina, L., Koelmans, A. A., Kukulka, T., Laufkötter, C., Lebreton, L., Lobelle, D., Maes, C., Martinez-Vicente, V., Maqueda M. A. M., Poulain-Zarcos, M., Rodríguez, E., Ryan, P. G., Shanks, A. L., Shim, W. J., Suaria, G., Thiel, M., Van Der Bremer, T. S., Wichmann, D. 2020. The physical oceanography of the transport of floating marine debris. *Environmental Research Letters*, 15(2), 023003.

Van Sebille, E., Griffies, S . M ., A bernathey, R ., A dams, T. P., Berloff, P., Biastoch, A., Blanke, B., Chassignet, E. P., Cheng, Y., Cotter, C. J., Deleersnijder, E., Döös, K., Drake, H. F., Drijfhout, S., Gary, S. F., Heemink, A. W., Kjellsson, J., Koszalka, I. M., Lange, M., Lique, C., Macgilchrist, G. A., Marsh, R., May-Orga Adame, C. G., Mcadam, R., Nencioli, F., Paris, C. B., Piggott, M. D., Polton, J. A., Rühs, S., Shah, S. H. A. M., Thomas, M. D., Wang, J., Wolfram, P. J., Zanna, L. & Zika, J. D. 2018. Lagrangian ocean analysis: Fundamentals and practices. *Ocean Modelling*, 121, 49–75. DOI: https://doi.org/10.1016/j.ocemod.2017.11.008

Visuri, O., Wierink, G. A. & Alopaeus, V. 2012. Investigation of drag models in cfd modeling and comparison to experiments of liquid–solid fluidized systems, *International Journal of Mineral Processing*, 104, 58–70. DOI: https://doi.org/10.1016/j.minpro.2011.12.006

Weckhuysen, B., Have, I. T., Meirer, F., Oord, R., Zettler, E., Sebille, E. V. & Amaral-Zettler, L. 2021. Nanoscale Infrared Spectroscopy Reveals Nanoplastics at 5000 m Depth in the South Atlantic Ocean, *preprint*, In Review. DOI: https://doi.org/10.21203/rs.3.rs-955379/v1

Woodall, L. C., Sanchez-Vidal, A., Canals, M., Paterson, G. L., Coppock, R., Sleight, V., Calafat, A., Rogers, A. D., Narayanaswamy, B. E. & Thompson, R. C. 2014. The deep sea is a major sink for microplastic debris. *Royal Society Open Science*, 1(4): 140317. DOI: https://doi.org/10.1098/rsos.140317

Zalasiewicz, J., Waters, C. N., Ivar do Sul, J. A., Corcoran, P. L., Barnosky, A. D., Cearreta, A., Edgeworth, M., Gałuszka, A., Jeandel, C., Leinfelder, R., Mc-Neill, J. R., Steffen, W., Summerhayes, C., Wagreich, M., Williams, M., Wolfe, A. P. & Yonan, Y. 2016. The geological cycle of plastics and their use as a stratigraphic indicator of the Anthropocene. *Anthropocene*, 13, 4–17. DOI: https://doi.org/10.1016/j.ancene.2016.01.002

Zhao, S., Zettler, E. R., Bos, R. P., Lin, P., Amaral-Zettler, L. A. & Mincer, T. J. 2022. Large quantities of small microplastics permeate the surface ocean to abyssal depths in the South Atlantic Gyre. *Global Change Biology,* 28(9), 2991–3006. DOI: https://doi.org/10.1111/gcb.16089